Identification of the sensory properties of image-based multi-axis force/torque sensors

Nassr Al-Baradoni* and Peter Groche, Institute for Production Engineering and Forming Machines, Technical University of Darmstadt, 64287 Darmstadt, Germany
* Correspondence author, al-baradoni@ptu.tu-darmstadt.de

Abstract

A novel image-based sensor concept for the detection of multi-axial forces/torques has been introduced by the authors in previous publications. The sensor concept is capable of detecting multiaxial loads in a single image and uniquely identifying all load components. In the present work, the sensory properties of the image-based multi-axis force-torque sensor are investigated in more detail. On the one hand, it compares the measurement resolution and measurement ranges as essential properties of a force/torque sensor with dominate strain gauge-based ones. Moreover, the measuring dynamics of the sensor are addressed and Deep Learning approaches are investigated to enhance the computationally intensive analysis process of the image data of such sensors.

1 Introduction

Multi-axis force/torque sensors are capable of sensing the magnitude and direction of acting forces. So far, mainly robotics makes use these types of sensors, e.g. on grippers or tools on the end effector. Due to the advancing digitalization as well as the growing implementation of process monitoring approaches, the employment of force and/or torque sensors is becoming more and more important in many processes. A good example of this are forming processes, where deviations in force distributions due to tool wear lead to variations in the workpiece characteristics. To monitor the force distribution during the shear cutting process, Groche et al. implemented spatially distributed uniaxial force sensors in the tool assembly [1]. In a similar approach, Kim et al. implemented spatially distributed uniaxial force sensors on the guidance column of the forging die to detect a non-symmetrical distribution of the process force during the forging process [2]. However, despite growing demand, the high cost of multi-axis force/torque sensors prevents a widespread implementation in many processes. According to Lee et al, despite their usefulness and necessity, multi-axis force/torque sensors are reluctantly used because of their high cost. They reported that there is a tendency to avoid multiaxial force sensors unless their absence would have a serious impact on performance [3]. In addition to research on reducing the cost of strain gauge based sensors, such as the reduction of the cost of the required electronics by using a multiplexer between the strain gauge and the voltage amplifiers [4], many studies have investigated alternative measurement concepts for cost effective multi-axis force/torque measurement. Here, optical-based sensors gain a special attraction in terms of cost-efficiency and simplicity of design. Most of this work is based on measuring the change of light intensity due to the deformation of a structure under loads in order to determine the acting load and their directions, as stated in [5], [6]. Meanwhile, there is a commercial optical-based force/torque sensor from OnRobot [7]. However, the measuring resolution of the intensity-based force sensors with respect to the needed deformation of the host structure is far behind the performance achievable by strain gauge-based or piezoelectric sensors. This means that a larger deformation of the host structure is required to measure a signal change. According to Berkovic et al., optical measuring of small deformations or distance changes with higher resolution, i.e. in the range of one micrometer, requires relatively expensive and complex measurement techniques such as interferometry or confocal scanning [8], which no longer meet the goal of cost-effective alternatives.

As part of our research to create low-cost multi-axial force/torque measuring load-bearing structures, an image-based measuring concept capable of capturing a three dimensional displacement in a single image has been developed. Based on digital image correlation DIC, the measuring concept can detect displacements in the range of less than one micrometer [9]. In addition, the sensor body can consist of a simple cylindrical structure, in contrast to the complex design requirements of strain gauge based sensors. In this paper, we investigate which properties the sensor can offer compared to strain gauge-based sensors. To increase the measuring dynamics of the sensor, the potential of applying deep learning approaches in image analysis is investigated. After a description of the sensor design the measurement resolution is investigated experimentally. Subsequently, the measurement dynamics of the DIC algorithm is discussed and a CNN model for image processing is presented. At the end, the results of the paper are summarized.

ISBN 978-3-8007-5835-7

2 Methods

2.1 The image-based force/torque sensor

The developed measuring concept (**Figure 1**) is based on the detection of the relative displacement between two planes on a host structure under load. The first plane comprises a carrier disk on which an image sensor including lenses is mounted. The second one involves an optical object attached to a carrier disk. Both carrier disks are fixed at a certain distance inside the host structure. The object is divided into two parts and consists of directly viewed and mirrored viewed patterns. The directly observed pattern (red beam in **Fig. 1**) contains information about displacements or rotation of the two carrying disks under load (bending or torsion), also so-called in-plane displacements, due to the parallel arrangement to the image sensor. The mirrored pattern (green beam in **Fig. 1**), on the other hand, is mirrored to include axial displacements or distance changes between the two planes, also called out-of-plane displacements. The pattern comprises a photomask with transparent regions defined in size and position. The use of such photomasks aims to increase the contrast and thus the measurement resolution and to reduce the calculation time

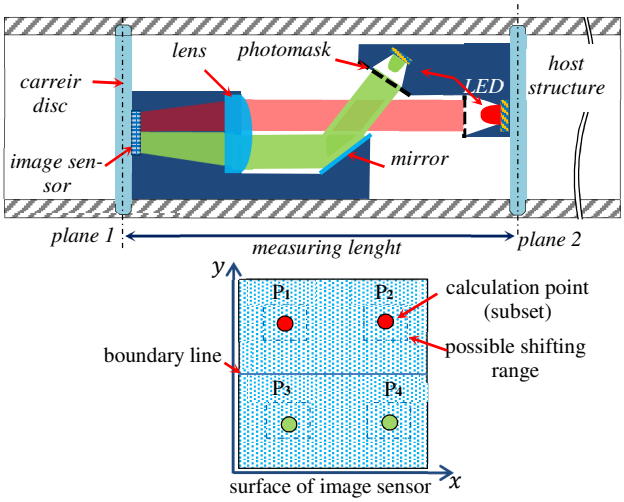

Figure 1 Principle of function for multi-axis force/torque measurement

during image analysis to four evaluation points in the entire image [9].

Figure 1 illustrates the design of the sensor. The lower part of the figure shows how the back-illuminated photomask leads to only four processing points on the sensor surface. The two upper points contain information about the displacements of the mirrored beam and the two lower ones about the direct beam. Furthermore, it can be seen that only the search process of the points is limited to specified displacement fields, which are determined by the maximum possible load on the host structure and the resulting maximum relative displacement between the two planes. When the structure is loaded, the displacement is calculated at two points in each pattern, from which the different loads are calculated based on geometric relationships [9].

In the experimental study of the present work, the sensor parts are installed in a steel cylinder structure with a measuring length of 108 mm and a diameter of 110 mm with a wall thickness of 2 mm. For the optical system, a CMOS image sensor (OV5647) was used with a pixel size of 1.4 µm and a sensing area of 2592 x 1944 pixels ~ 3.6 x 2.7 mm. The lens system was designed to have a magnification factor of 3.4. The sensor is configured for the maximum expected displacements at the maximal permissible loads of the mechanical structure of 100 kN axial force, 31 kN bending force and 4 k Nm torsional moment. These values determine the measuring ranges of the individual measuring axes. On the other side, the most critical feature of the image-based sensor compared to the strain gauge-based one is the measurement resolution. This is defined by the smallest detectable displacement and can be mainly influenced by the pixel size in the image sensor and by the optical magnification. Assuming an evaluation accuracy of up to one px on the image processing, this displacement results in the theoretically smallest measurable loads of: 318 N for the axial force, 125 N for the bending force and 374 Nm for the torque. Here, the maximum loads cause the maximum displacements of: 350 px at Fz of 100 kN, 250 px at bending force of 31 kN and a rotational displacement of up to 15 pixels at a torque of 4 kNm. The displacements are calculated via the DIC algorithm with a subpixel registration of 0.1 pixel using the cores-fine search method according to [10].

2.2 Evaluation of the measuring resolution

The measuring resolution is experimentally determined for each measurement axis. For this purpose, the sensor is mounted in a developed test bench (**Figure 2**) with a strain gauge-based reference sensor from HBM (K-MCS10-025).

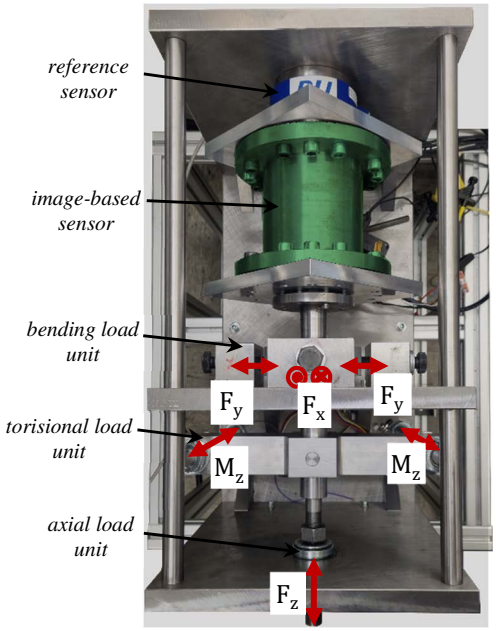

Figure 2 Developed test bench for multiaxial sensor loading

The loads F_x, F_y, M_z and F_z are then separately applied. The maximum permissible loads F_{xy} 5 kN, M_z 250 Nm and F_z 15 kN for the reference sensor were applied and released in 20 steps in both measuring directions. Due to the long lever arm between the bending load unit and the reference sensor in the developed test bench, the maximum permissible bending moments M_{xy} in the reference sensor of 350 Nm were already reached at bending forces F_{xy} of to 1 kN. Therefore, the load range of the bending forces is reduced to 1 kN.

Due to the high stiffness of the structure and the low maximum torque of the reference sensor, an additional torsion test was performed on a torque calibration test bench with a torque sensor (HBM TB2 1 kNm) loaded in the range of ± 1 k Nm.

As shown in **Figure 2**, the loads F_x, F_y, M_z, F_z are manually adjusted by the bolt fastening in decoupled loading units.

2.2.1 Bending forces F_x and F_y

When loading the sensor with the bending forces F_x and F_y, displacements at the points P_1 and P_2 were calculated. First, these displacements are transformed via coordinate transformation from the coordinate system of the image sensor $(x - y)$ to the coordinate system of the reference sensor $(\tilde{x} - \tilde{y})$. This way, the displacement in the $\tilde{x}$-axis becomes a linear function of F_x and the displacement in the $\tilde{y}$-axis becomes a linear function of F_y. **Figures 3** and **4** show the calculated displacements in relation to the forces measured by the reference sensor.

As can be seen in both **Figures 3** and **4**, a linear behaviour between the displacements and the bending forces can be observed. A maximum deviation of 104 N was determined for F_x and 100 N for F_y. In respect to their measuring range of 31 kN, a deviation of about 0.33 % can be determined. However, this linear behaviour assumes that the tilt of plane 1 to plane 2 is negligible.

2.2.2 Torque M_z

During data evaluation, it was observed, that there is no shift at points P_1 and P_2 for torques up to 1 kNm. This is

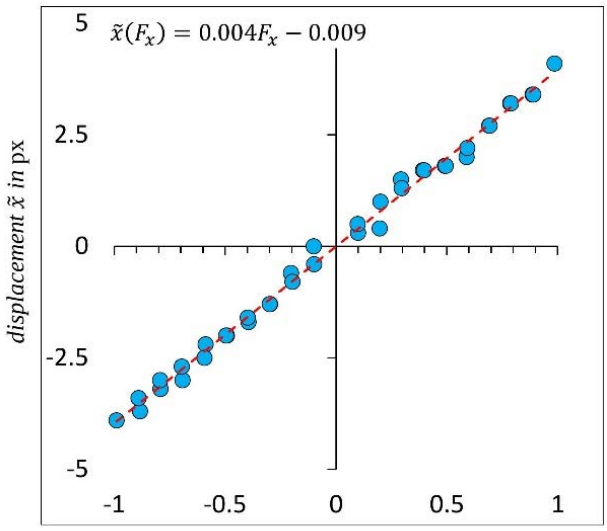

Figure 3 Displacement at P_1 and P_2 caused by F_x

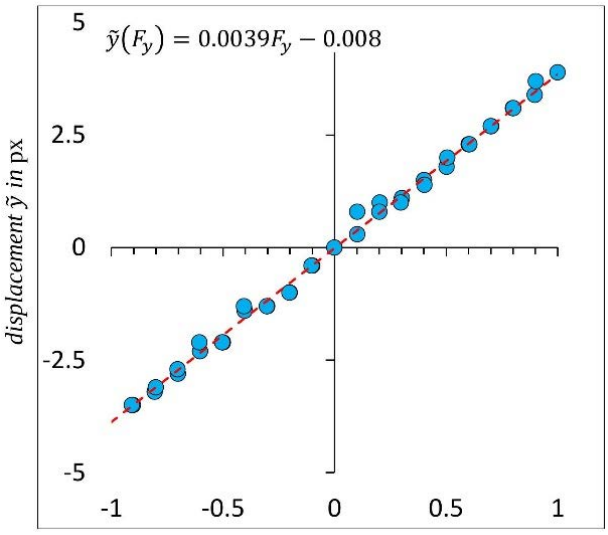

Figure 4 Displacement at P_1 and P_2 caused by F_y

caused by the high stiffness of the structure and the very small distance between the points P_1 and P_2, which is set to about 800 pixels. Taking into account the optical magnification of 3.4 and the pixel size of 1.4 µm, this distance results in a distance of 0.33 mm. However, since a distance between the upper pattern (green beam in **Figure 1**) and the mirror is about 13 mm, a detectable displacement of the points P_3 and P_4 along the x -axis was observed. **Figure 5** shows the detected displacement at P_3 and P_4 along the x -coordinates of the image sensor under the applied torque load.

The green boxes in **Figure 5** represent the load curve on the developed test bench with the reference sensor at a torsional load between ± 250 Nm. The blue circles represent the loads in the torque calibration system with a torsional load between ± 1 kNm.

The measured data show a maximum deviation of 95 Nm. With reference to a measuring range of 4 kNm, this results in a deviation of 2.5 %.

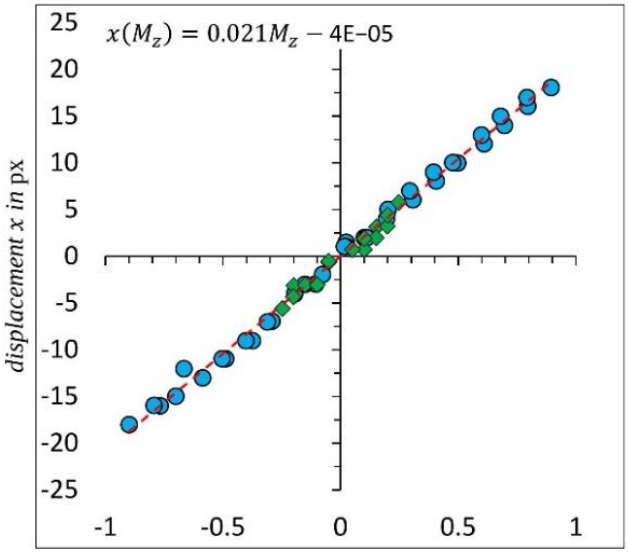

Figure 5 Displacement at P_3 and P_4 caused by M_z

2.2.3 Axial force Fz

When the host structure is subjected to an axial load Fz, the distance between the two measuring planes plane1 and plane2 (**Figure 1**) changes. This causes no change in points 1 and 2, but the mirrored beam P_3 and P_4 is shifted along the y -axis of the image sensor. **Figure 6** shows the calculated displacement at P_3 and P_4, occurring along the y -axis of the image sensor at an axial load between ±15 kN.

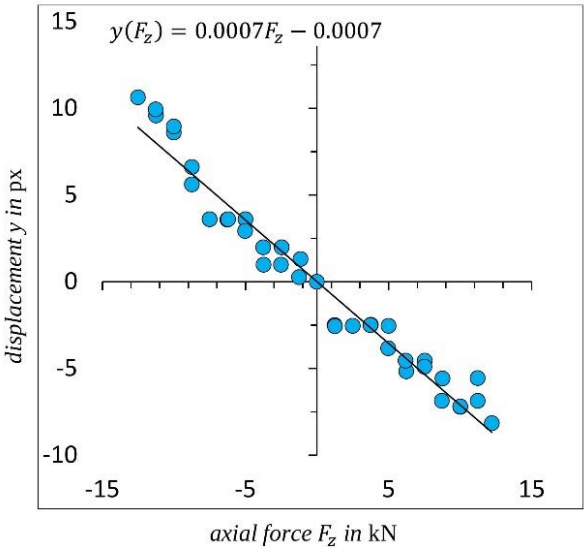

Figure 6 Displacement at P_3 and P_4 caused by F_y

Figure 6 shows a linear and more scattered trend compared to the results for F_x, F_y and M_z. A maximum deviation of 3.7 kN is found. With respect to the measurement range, a deviation of 3.7 % is calculated.

2.2.4 Comparison of the measurement resolution to strain gauge-based sensors

The deforming body in strain gauge-based sensors has different geometric shapes depending on the system requirements such as required load conditions or measuring ranges. The highest measurement resolutions are achieved by means of the bending principle, while the largest measurement ranges are available for tension/compression transducers [11]. The following table shows the measurement resolution achieved in the developed sensor in comparison with the used reference sensor (HBM: K-MCS10-025) and another sensor (HBM:MSC10-100), which has measurement ranges of F_z 100 kN, F_{xy} 20 kN, M_z 15 kNm. The deviations are calculated by dividing the maximum error to the measuring range:

Table 1 Comparison of the measurement resolution of the image-based and strain gauge-based sensors

load	imaged-based	used HBM reference Sensor	HBM-MSC10-100
F_x	0.33 %	0.12 %	0.026 %
F_y	0,33 %	0.12 %	0.026 %
M_z	2,5 %	0.34 %	0.056 %
F_z	3,7 %	0.06 %	0.015 %

2.3 The image analysis process

A major shortcoming of image-based measuring concepts compared to strain gauge measuring methods or optical ones based on light intensity detection is the low measuring dynamics, due to the required computationally expensive image-processing step. The computation time increases almost exponentially with the size of the search field and the degree of subpixel registration.

Figure 7 shows an example of the computation CPU time as a function of the degree of subpixel registration for a subset size of 40 x 40 pixels and a search field of 8 (solid line) and of 40 pixels (dashed line). The used notebook has a 2.4 GHz Intel Core 2 Duo processor and 4 GB 1067 MHz DDR3 RAM.

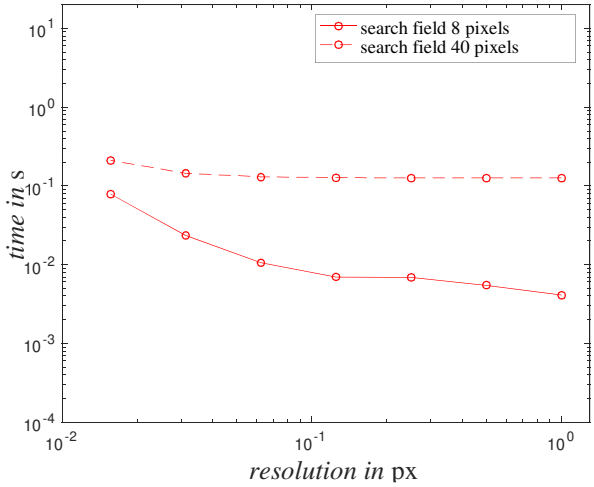

Figure 7 Required calculation time depending on the subpixel registration

Figure 7 shows that the smaller the search field, the faster the image processing. If high subpixel registration is used, the processing time increases almost exponentially for smaller search fields. For a search field of 40 pixels, the processing time over the degrees of subpixel registration is almost steady. This is due to the fact, that only the significant regions of the image where the correlation is highest are considered for image interpolation. Therefore, the smaller the search field, the greater the effect of increasing subpixel registration. For the evaluation of 4 points with a size of 40 pixels and in a field of 40 x 40, a time of 2.5 s would be required without subpixel registration.

For a maximum displacement of only 8 pixels, only 0.12 s computing time is required. This presents a challenge when high optical magnifications are also deployed. Generally, the smaller the features, the higher the displacement sensitivity. Since the fabrication of speckle-sized features (2-20 µm) by UV photolithography is very expensive, the cost increases as the speckle size becomes smaller [10].

For alternative image processing methods, the CNN models seem to be the most suitable. However, in order to train a network, a large amount of data is usually required, which is an obstacle for the sensor technology that generates only a limited amount of data during the calibration process.

ISBN 978-3-8007-5835-7

2.3.1 CNN based displacement computation

In this work, we have investigated the design of a simplified CNN, which can achieve the accuracy with a small amount of training data. First, 72 images are acquired at different loads and evaluated using the DIC algorithm. With this data and the displacements calculated by DIC, a CNN is trained. This way, the CNN model will be able to replace the DIC in calculation of the displacements with less computation time. Since CNNs have high performance in classification tasks [12], the considered problem is reduced to a classification problem. As in the current data the displacements in the image are less than 100 pixels and have an evaluation resolution of up to one decimal digit, the CNN was divided into three stages. The first level of F-CNN determines the displacements in the 10s scale. The second level of S-CNN determines the displacements in single digits and the last level, T-CNN, determines the displacements in the decimal digits. Each level includes 10 classes, which classifies the displacements between 1 and 10. To keep the complexity of the network to be created and thus the required amount of training data as low as possible, the algorithm is designed to calculate displacements in one direction only. In order to determine displacements in all directions, each image is rotated by 0°, 90°, 180°, and 270°, the displacement is calculated each time and assigned to the axis depending on the rotation. The CNN then recognizes the displacements in all directions, i. e. as displacement in positive x-direction. The resulting CNN has three basic units and three fully connected layers. Each basic unit contains two convolution layers. Each convolution has a kernel size of 5×5 pixels. The convolution in the first Basic Unit contains 16 kernels, in the second Basic Unit 32 kernels and in the third 64 kernels. In **Figure 8**, the accuracy is determined by the evaluation for each classification level and the resulting computation time as a function of the number of fully interconnected layers. The first number in the square brackets is the number of layers and the second number is the accuracy or the calculation time, respectively.

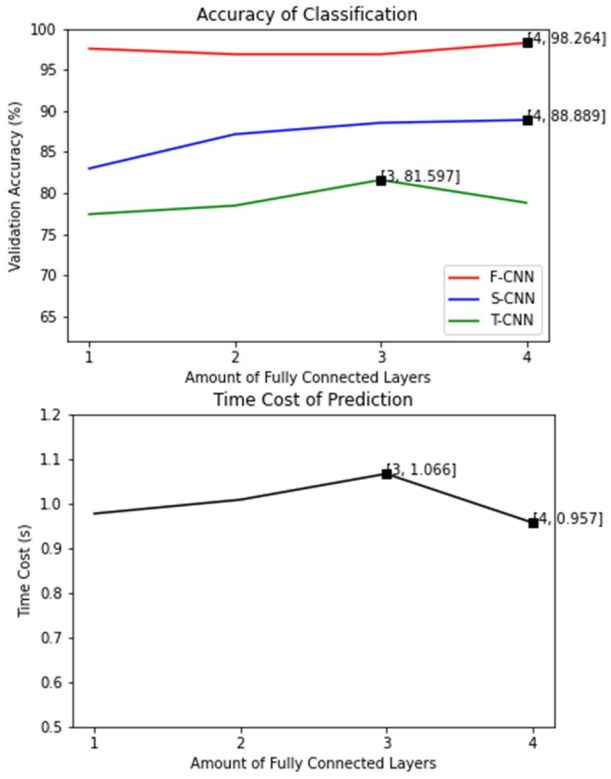

Figure 8 Achieved accuracy and needed calculation time of the created CNN to calculate the displacements

As can be seen in **Figure 8**, the created CNN, the F-CNN, achieves an accuracy of classification of 97.569 %, the S-CNN 89.584 % and the T-CNN 82.636 %. The training time required for the entire CNN structure is 1130.314 s. For the evaluation of an image consisting of four subsets of 80 pixels, the required CPU time is 0.87 s. The maximum error related to the maximal displacement is 5.066 %. The error results mainly from the calculation of the displacement in the decimal point and can be partly attributed to the deviation in the DIC algorithm.

3 Conclusion

In this paper, an image-based multiaxial force/torque sensor is presented and its essential properties in terms of measuring resolution and measurement range are compared with the market-dominant strain gauge-based sensors. Compared to the existing investigated and intensity-based optical force/torque sensors in the state of the art, the developed sensor appears to be a promising cost-effective alternative regarding the achievable measuring resolution. However, the achieved resolution is still far behind the performance of strain gauge based sensors, as shown in (**Table 1**). An increase of the measurement resolution can mainly be obtained by increasing the optical magnification. In this case, the system design must be optimized to avoid the negative effect of the optical magnification on the measurement resolution on the torque.

Due to the relatively time-consuming image processing, the sensor has a low measurement dynamic. Initial investigations into the use of CNN in the image evaluation process show potential for increasing the measuring dynamics through the use of CNN algorithms.

Future work will investigate the potential for using CNN throughout the evaluation and calibration process of the sensor behaviour.

ISBN 978-3-8007-5835-7

4 Literature

[1] P. Groche, J. Hohmann, and D. Übelacker, "Overview and comparison of different sensor positions and measuring methods for the process force measurement in stamping operations," *Measurement*, vol. 135, pp. 122–130, Mar. 2019.

[2] S. Y. Kim, A. Ebina, A. Sano, and S. Kubota, "Monitoring of process and tool status in forging process by using bolt type piezo-sensor," *Procedia Manufacturing*, 01-Jan-2018. .

[3] D. H. Lee, U. Kim, H. Jung, and H. R. Choi, "A capacitive-type novel six-axis force/torque sensor for robotic applications," *IEEE Sensors Journal*, vol. 16, no. 8, pp. 2290–2299, Apr. 2016.

[4] P. Billeschou, C. Albertsen, J. C. Larsen, and P. Manoonpong, "A Low-Cost, Compact, Sealed, Three-Axis Force/Torque Sensor for Walking Robots," *IEEE Sensors Journal*, vol. 21, no. 7, pp. 8916–8926, Apr. 2021.

[5] Á. Tar and G. Cserey, "Development of a low cost 3D optical compliant tactile force sensor," in *IEEE/ASME International Conference on Advanced Intelligent Mechatronics, AIM*, 2011.

[6] H. Xie, A. Jiang, L. Seneviratne, and K. Althoefer, "Pixel-based optical fiber tactile force sensor for robot manipulation," in *Proceedings of IEEE Sensors*, 2012.

[7] "Optical force-/torque sensor." [Online]. Available: https://onrobot.com/de/produkte/hex-6-achsiger-kraft-drehmoment-sensor.

[8] G. Berkovic and E. Shafir, "Optical methods for distance and displacement measurements," *Advances in Optics and Photonics*, 2012.

[9] N. Al-Baradoni and P. Groche, "Sensor Integrated Load-Bearing Structures: Measuring Axis Extension with DIC-Based Transducers," *Sensors 2021, Vol. 21, Page 4104*, vol. 21, no. 12, p. 4104, Jun. 2021.

[10] S. Simončič, M. Kompolšek, and P. Podržaj, "AN ADVANCED COARSE-FINE SEARCH APPROACH FOR DIGITAL IMAGE CORRELATION APPLICATIONS," *Facta Universitatis, Series: Mechanical Engineering*, vol. 14, no. 1, pp. 63–73, Apr. 2016.

[11] M. Stahl-Offergeld, "Robuste dreidimensionale Hall-Sensoren für mehrachsige Positionsmesssysteme," in *Aktuelle Berichte aus der Mikrosystemtechnik - Recent Developments in MEMS*, 2011.

[12] J. Wang, Y. Yang, J. Mao, Z. Huang, C. Huang, and W. Xu, "CNN-RNN: A Unified Framework for Multi-label Image Classification," in *Proceedings of the IEEE Computer Society Conference on Computer Vision and Pattern Recognition*, 2016, vol. 2016-Decem, pp. 2285–2294.

5 Acknowledgments

- This research is funded by the Deutsche Forschungsgemeinschaft (DFG, German Research Foundation)—Project number 460244297. The authors would like to thank the German Research Foundation for founding and supporting this research project.
- The authors would like to thank Sven Winter for his support in investigating DIC-based image processing in the context of his master thesis and Boxuan Zhang and Frederik Emanuel Bialek for their support in investigating CNN-based image processing in the context of a student project.

